





Tissue-Specific T_2^* Biomarkers in Patellar Tendinopathy by Subregional Quantification Using 3D Ultrashort Echo Time MRI

Stephan J. Breda, MD,^{1,2}  Dirk H.J. Poot, PhD,¹ Dorottya Papp, MSc,¹ Bas A. de Vries, MSc,¹ Gyula Kotek, PhD,¹ Gabriel P. Krestin, MD, PhD,¹ Juan A. Hernández-Tamames, PhD,¹ Robert-Jan de Vos, MD, PhD,² and Edwin H.G. Oei, MD, PhD^{1*} 

Background: Quantitative MRI of patellar tendinopathy (PT) can be challenging due to spatial variation of T_2^* relaxation times. **Purpose:** 1) To compare T_2^* quantification using a standard approach with analysis in specific tissue compartments of the patellar tendon. 2) To evaluate test–retest reliability of different methods for fitting ultrashort echo time (UTE)-relaxometry data.

Study Type: Prospective.

Subjects: Sixty-five athletes with PT.

Field Strength/Sequence: 3D UTE scans covering the patellar tendon were acquired using a 3.0T scanner and a 16-channel surface coil.

Assessment: Voxelwise median T_2^* was quantified with monoexponential, fractional-order, and biexponential fitting. We applied two methods for T_2^* analysis: first, a standard approach by analyzing all voxels covering the proximal patellar tendon. Second, within subregions of the patellar tendon, by using thresholds on biexponential fitting parameter percentage short T_2^* (0–30% for mostly long T_2^* , 30–60% for mixed T_2^* , and 60–100% for mostly short T_2^*).

Statistical Tests: Average test–retest reliability was assessed in three athletes using coefficients-of-variation (CV) and coefficients-of-repeatability (CR).

Results: With standard image analysis, we found a median [interquartile range, IQR] monoexponential T_2^* of 6.43 msec [4.32–8.55] and fractional order T_2^* 4.39 msec [3.06–5.78]. The percentage of short T_2^* components was 52.9% [35.5–69.6]. Subregional monoexponential T_2^* was 13.78 msec [12.11–16.46], 7.65 msec [6.49–8.61], and 3.05 msec [2.52–3.60] and fractional order T_2^* 11.82 msec [10.09–14.44], 5.14 msec [4.25–5.96], and 2.19 msec [1.82–2.64] for 0–30%, 30–60%, and 60–100% short T_2^* , respectively. Biexponential component short T_2^* was 1.693 msec [1.417–2.003] for tissue with mostly short T_2^* and long T_2^* of 15.79 msec [13.47–18.61] for mostly long T_2^* . The average CR (CV) was 2 msec (15%), 2 msec (19%) and 10% (22%) for monoexponential, fractional order and percentage short T_2^* , respectively.

Data Conclusion: Patellar tendinopathy is characterized by regional variability in binding states of water. Quantitative multicompartiment T_2^* analysis in PT can be facilitated using a voxel selection method based on using biexponential fitting parameters.

Level of Evidence: 1

Technical Efficacy Stage: 1

J. MAGN. RESON. IMAGING 2020.

Patellar tendinopathy (PT) is an overuse tendon injury that is typically observed in athletes performing repetitive jumping activities, such as volleyball and basketball.¹ PT results in load-related anterior knee pain at the site of the patellar tendon attachment to the patella.² Pain in PT is often chronic, resulting in decreased activity levels and in

View this article online at wileyonlinelibrary.com. DOI: 10.1002/jmri.27108

Received Jan 10, 2020, Accepted for publication Feb 13, 2020.

*Address reprint request to: E.O., Doctor Molewaterplein 40, 3015 GD Rotterdam, The Netherlands. Email: e.oei@erasmusmc.nl

From the ¹Department of Radiology & Nuclear Medicine, Erasmus MC University Medical Center Rotterdam, Rotterdam, The Netherlands; and ²Department of Orthopedics and Sports Medicine, Erasmus MC University Medical Center Rotterdam, Rotterdam, The Netherlands

This is an open access article under the terms of the Creative Commons Attribution-NonCommercial-NoDerivs License, which permits use and distribution in any medium, provided the original work is properly cited, the use is non-commercial and no modifications or adaptations are made.

more than half of the patients in decreased work participation.^{3,4}

On histopathological analysis, PT is associated with degenerative tissue changes that are typically located at the posterior aspect of the proximal patellar tendon.⁵ Histopathological features of tendinopathy include collagen disorganization and fiber separation with increased proteoglycans and associated glycosaminoglycan (GAG) side chains within the extracellular matrix.⁶ This accumulation of GAGs in the proximal patellar tendon leads to an increased water content within the extracellular matrix, because of the highly negative charge of GAGs with a strong potential for binding water.⁷ A simplified model to characterize the different water pools within the patellar tendon is the bicomponent model.⁸ Water in voxels that contain highly organized collagen is primarily in a “bound” state, thereby restricting the motion of water molecules by stronger spin–spin interactions, thus resulting in shorter T_2^* relaxation times (reflecting the macromolecular bound water compartment). Loosely bound water or even “free” water pools result in a longer T_2^* .⁹ The different water pools reflect specific tissue compartments within the patellar tendon.¹⁰ Quantifying these different water pools may be clinically relevant, as a previous histological study in patients undergoing surgery demonstrated an association between levels of GAGs and severity of PT symptoms.¹¹

Currently, imaging in PT with morphologic magnetic resonance imaging (MRI) techniques is of limited value, because the diagnosis of PT is primarily made clinically.¹² These MR techniques are sensitive for detecting increased signal in the proximal patellar tendon, representing an elevated water content.¹³ However, conventional MRI of tendons is typically limited for the assessment of different water pools in the patellar tendon due to the fast free induction decay of collagen.¹² The short T_2^* -components in tendons will consequently appear dark using conventional sequences. Ultrashort echo time (UTE) sequences are sensitive to different water pools in the patellar tendon.¹⁴ Quantitative T_2^* mapping is performed by multiple-spin-echo decay analysis using voxelwise fitting methods.¹⁵ Monoexponential, or single-component fitting is a robust method to describe signal decay in which the MR signal in each voxel is assumed to result from only a single component. However, residual signal is observed using this method, indicating that the signal from each voxel consists of different components.⁹ In order to gain insight in this subpixel composition, the biexponential model has been introduced to reveal both short and long water components in each voxel.¹⁶ Fractional order fitting has also been proposed as an alternative mathematical model to describe relaxation in complex heterogeneous tissues and is derived from a nonlinear generalization of the Bloch equations.¹⁷

The primary aim of this study, therefore, was to quantify T_2^* in specific tissue compartments by optimizing the image analysis approach in which voxels containing comparable water

pools are automatically selected. Moreover, we compared different methods for fitting T_2^* relaxometry data and evaluated test–retest reliability of the T_2^* quantification.

Materials and Methods

This single-center prospective observational study was approved by the local Institutional Review Board (decision number: NL58512.078.16). Participants provided written informed consent prior to inclusion. We performed cross-sectional analysis of baseline data from a prospective trial investigating the effectiveness of two different exercise programs for PT.

Study Population

Participants were consecutively recruited. To be eligible for inclusion, athletes aged 18–35 years must have a clinical diagnosis of patellar tendinopathy that was confirmed by ultrasound and had to perform sports involving frequent jumping or cutting maneuvers for at least 3 times per week. The activity level was assessed using the Cincinnati Sports Activity Scale (CSAS), which incorporates both frequency of sports participation and the general types of forces experienced by the lower extremity during the sport.¹⁸ The Victorian Institute of Sports Assessment questionnaire for patellar tendons (VISA-P) was administered to measure symptoms, function, and ability to play sports.¹⁹ Criteria for the clinical diagnosis were: 1) a history of localized pain at the inferior pole of the patella, 2) recognizable pain on palpation over the patellar tendon, and 3) injury pain on the single leg squat. Clinical evaluation was performed by a sports physician (R.V.) with 10 years of experience in athlete care. The clinical evaluation was followed by an ultrasound examination (LOGIQ E9, GE Healthcare, Chicago, IL) of the patellar tendon performed by one trained examiner (S.B.: radiologist-in-training with 5 years’ experience), and was regarded positive for PT when there was the presence of structural and/or hypoechoic changes and/or tendon thickening (anterior–posterior diameter >6 mm) and/or the presence of intratendinous power Doppler flow.²⁰ Other eligibility criteria are mentioned in the preregistered trial protocol, ClinicalTrials.gov (ID: NCT02938143).

MR Examination

MRI was performed with a 3.0T clinical scanner (Discovery MR750, GE Healthcare, Waukesha, WI) using a 16-channel small flexible coil (NeoCoil, Pewaukee, WI). For stabilization of the knee, a support device was used in combination with a plastic cylindrical tube and foam padding to keep the knee flexed at 30° (Fig. 1). The center-spot of the coil was aligned with the inferior patellar border. Acquisition was initiated with a sagittal 3D proton-density (PD) fast spin echo sequence of the knee, which was subsequently used to create precise localizer images to plan further acquisitions aligned with the direction of the collagen fibers of the patellar tendon. The patellar tendon was scanned in the axial plane using 3D-UTE-Cones (GE Healthcare), which is a gradient-echo-based acquisition using radial readout of the k -space. A total of 16 echoes were acquired in four separate multiecho sequences containing four echoes in interleaved order. For each multiecho acquisition, the same repetition time (TR) was used. Total acquisition time was 65 minutes. The full protocol for sequence parameters in this study is listed in Table 1.



FIGURE 1: Standardized positioning of the knee during MRI. Illustrated is the positioning of the 16-channel flexible coil in combination with the support device that was used for knee stabilization and standardization of the knee flexion angle.

The MR examination was repeated in three athletes with patellar tendinopathy, who returned the next day for the purpose of measuring reproducibility.

Image Preparation

Image registration was performed in order to perform a spatial one-to-one mapping from voxels between the different UTE acquisitions with in-house-developed registration tools (Elastix v. 4.8, Rotterdam,

The Netherlands)^{21,22} and MatLab software (R2015b; MathWorks, Natick, MA). Initially, a rigid registration to correct for rotation and translation was performed on the entire knee to compensate for motion in between multiecho scans and separate visits (for the test-retest subjects). Second, a groupwise nonlinear refinement registration was performed inside a volume of interest covering the patellar tendon.²² The volume of interest was constructed from regions of interest drawn on three orthogonal views.

TABLE 1. Imaging Protocol

Sequence	3D PD Cube	3D PD Cube FS	3D ME-UTE
Matrix	384 × 384	384 × 384	252 × 252
Scan plane	Sagittal	Sagittal	Axial oblique
Fat saturation	—	Fat	2 excitations per FS
FOV (cm)	15.0	15.0	15.0
Resolution (mm)	0.4 × 0.4 × 1.0	0.4 × 0.4 × 1.0	0.6 × 0.6 × 1.5
Slice thickness (mm)	1.0	1.0	1.5
Number of slices	120	120	60
TE (msec)	30.0	30.0	0.032/4.87/12.67/20.47 0.49/6.82/14.62/22.42 0.97/8.77/16.57/24.37 2.92/10.72/18.52/26.32
Number of echoes	1	1	16
TR (msec)	1200.0	1200.0	83.4
Flip angle (°)			17
Bandwidth (± kHz)	83.33	83.33	125
NEX	0.5	0.5	1.0
Scan time (mm:ss)	03:17	03:18	13:15

PD: proton density; ME: multiecho; UTE: ultrashort echo time; FOV: field-of-view; FS: fat saturation; TE: echo time; TR: repetition time; NEX: number of excitations.

Fitting Methods

Fitting of the UTE- T_2^* maps was performed using different models, namely, monoexponential, fractional order, and biexponential fitting. The T_2^* relaxation time was calculated using three different analysis algorithms, written in MatLab (R2015b; MathWorks).

Monoexponential T_2^* was fitted using the model²³:

$$M_m(TE) = a_0 \cdot e^{-\frac{TE}{T_2^*}} \quad (1)$$

where a_0 is the signal intensity at echo time (TE) = 0.

For biexponential T_2^* analysis, short T_2^* (T_{2S}^*) and long T_2^* (T_{2L}^*) components were fitted with the model²³:

$$M_b(TE) = b_0 \cdot e^{-\frac{TE}{T_{2S}^*}} + b_1 \cdot e^{-\frac{TE}{T_{2L}^*}} \quad (2)$$

where b_0 and b_1 are the magnetization of the short T_2^* and long T_2^* components, respectively.

The fractional order T_2^* relaxation model is given by¹⁷:

$$M_f(TE) = c_0 \cdot E_\alpha \left[-\left(\frac{TE}{T_2^*}\right)^\alpha \right] \quad (3)$$

where c_0 is the signal intensity at TE = 0 and E_α is the stretched Mittag-Leffler (M-L) function.²⁴ Note that for $\alpha = 1$, the M-L function is equivalent to the monoexponential function.

Fractional order fitting results in a stretched exponential T_2^* and a parameter " α " ($0 < \alpha < 1$) of the differential equation, which represents tissue heterogeneity.²⁵ In a voxel where $\alpha = 1$, the signal decay is best described as monoexponential and likely resulted from a single component. We used maximum likelihood estimation incorporating the Rician noise model for fitting the parameters of all methods.²⁶ This corrects for the noise-dependent bias in magnitude images.²⁷

Image Analysis

For calculation of median T_2^* relaxation times for the monoexponential, fractional order and biexponential fitting parameters in all subjects, we selected individual voxel data on 10 consecutive slices covering the proximal patellar tendon and for each separate slice of the proximal patellar tendon (Fig. 2). On each slice, we drew a mask that covered the outer margins of the patellar tendon, in order to analyze all voxels. The first region of interest (ROI) was drawn on the second slice distal from the patellar apex, to avoid partial volume effects of patellar bone. The subregional analysis in different tissue compartments was performed using thresholds on the percentage short T_2^* components, a parameter resulting from biexponential fitting. The thresholds resulted in an automatic selection of voxels within the mask of the patellar tendon, indicating the different tissue compartments. Based on the frequency distribution of the percentage short T_2^* components in a histogram, we defined 0–30% short T_2^* components for the highly hydrated degenerative tissue, which mainly contains long T_2^* components, 30–60% short T_2^* as the intermediate zone, and 60–100% for the ultrashort T_2^* components, such as the macromolecular bound water pools associated with aligned collagen. For quantitative analysis, only voxels within the initial mask covering the patellar tendon were selected.

Statistical Analysis

Statistical analysis was performed using IBM SPSS software v. 25 (Armonk, NY). Coefficients-of-variation (CV) were calculated using the root-mean-square method to assess test–retest reliability in each voxel. In this method, the CV is calculated voxelwise as the square root of the squared summed percentage differences in each voxel between the test and retest scans divided by the total number of voxels.²⁸ Within-subject variances were calculated as half the square of the differences between two scans.²⁹ Test–retest repeatability was assessed using coefficient-of-repeatability (CR), also referred to as smallest real

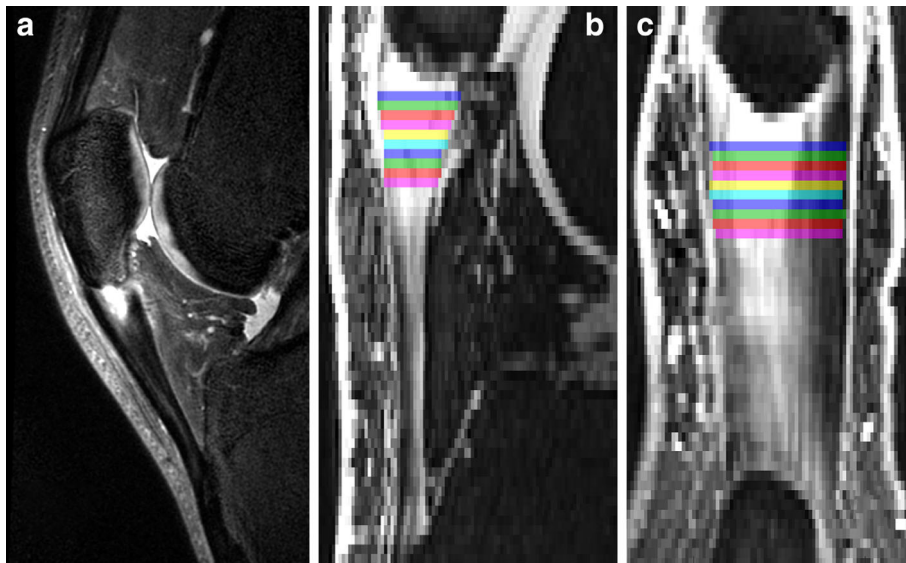


FIGURE 2: Locations for T_2^* quantification in patellar tendinopathy. (a) Sagittal PD Cube scan in an athlete with patellar tendinopathy and corresponding sagittal (b) and coronal (c) 3D-UTE scans (TE 4.87 msec). Color bars in the proximal patellar tendon represent the locations of the manually drawn masks in 10 slices for T_2^* quantification.

difference (SRD), calculated by multiplying the median within-subject standard deviation by 2.77 ($\sqrt{2}$ times 1.96).³⁰ Overall CV and CR were calculated as a mean over the three subjects. Normality of data was tested using the Shapiro–Wilk’s test. One-way analysis of variance (ANOVA) was used to determine whether there were statistically significant differences between the means of the subselected voxel groups. Differences between monoexponential fitting and fractional order fitting were assessed with Student’s *t*-test for normally distributed data and the Mann–Whitney *U*-test for nonnormally distributed data. Statistical significance was defined as $P < 0.05$.

Results

Study Population

In total, 76 athletes with clinically diagnosed and ultrasonographically confirmed PT were consecutively enrolled between January 2017 and June 2019. After exclusion of 11 subjects due to a change in our MR acquisition protocol during the study period, 65 athletes remained eligible for inclusion. Demographic characteristics of the study population are listed in Table 2.

Acquired 3D UTE-Cones Images

Figure 3a shows axial images of the knee in an athlete with patellar tendinopathy at all 16 echoes of the 3D UTE-Cones acquisitions, illustrating the fast signal decay occurring at the shortest echo times. Figure 3b–d shows signal intensity curves in the different tissue compartments of the patellar tendon (mostly long T₂*, mixed T₂*, and mostly short T₂*), fitted using monoexponential, biexponential, and fractional order models.

Image Analysis Using All Voxels

When using all voxels in all slices covering the proximal patellar tendon, we found a median [interquartile range, IQR] monoexponential T₂* of 6.43 msec [4.32–8.55] and fractional order T₂* 4.39 msec [3.06–5.78]. The overall percentage of short T₂* components was 52.9% [35.5–69.6]. Table 3 illustrates that the longest T₂* was found in the slice closest to the inferior patellar border (slice 1) and gradually decreased in the distal direction. Fractional order T₂* revealed a similar gradual decrease; however, fractional order T₂* was systematically lower than monoexponential T₂*. In addition, the percentage of short T₂* components was lowest in the slice closest to the inferior patellar border and gradually increased in the distal direction along the patellar tendon. The difference in median T₂* between the monoexponential and fractional order fitting in all voxels was statistically significant ($P < 0.001$).

Subregional Image Analysis Approach

In Fig. 4, a representative axial slice of an athlete with patellar tendinopathy is illustrated with the corresponding monoexponential, biexponential, and fractional-order T₂* maps. Voxels were selected with a percentage of short T₂* between 0–30%, 30–60%, and 60–100% based on histogram analysis (Fig. 5), and visually corresponded to degenerative tissue, transitional area between degenerative tissue and aligned

TABLE 2. Baseline Characteristics

Characteristic	<i>N</i> = 65
Mean age (years) ± SD	24.5 ± 3.8
No. of men (%)	50 (77)
Mean BMI (kg/m ²) ± SD	24.0 ± 2.9
Mean waist circumference (cm) ± SD	85.7 ± 9.4
Mean clinical score (VISA-P, 0–100) ± SD	55 ± 13
Median symptom duration (weeks) [IQR]	104 [40–182]
Sports activity scale (CSAS, 0–100)	<i>N</i> (%)
Level I (4 to 7 days/week)	
100	15 (23)
95	0 (0)
90	0 (0)
Level II (1 to 3 days/week)	
85	44 (68)
80	6 (9)

SD: standard deviation; IQR: interquartile range; BMI: body mass index; VISA-P: Victorian Institute of Sports Assessment questionnaire for patellar tendons; CSAS: Cincinnati Sports Activity Scale.

collagen, and aligned collagen in the patellar tendon, respectively. There were statistically significant differences in monoexponential and fractional order T₂* between all three different tissue compartments ($P < 0.001$). Table 4 illustrates that the longest T₂* was found in degenerative tissue (median monoexponential T₂* 13.78 msec, IQR [12.11–16.46], and fractional order T₂* 11.82 msec, IQR [10.09–14.44]) and the shortest T₂* in the voxels representing aligned collagen (median monoexponential T₂* 3.05 msec, IQR [2.52–3.60], and fractional order T₂* 2.19 msec [1.82–2.64]).

Test–Retest Reliability

Intravoxel test–retest CV and CR are listed in Table 5. Comparable reliability was found for monoexponential and fractional order fitting; we found an average CV of 15% and CR of 2 msec and an average CV of 19% and CR of 2 msec, respectively. The percentage short T₂* (biexponential fitting) had an average CV of 22% and CR of 10%. Average repeatability (CV) of biexponential T₂* quantification improved by using the subregional image analysis approach from 45% to 30% for short T₂* and from 25% to 11% for long T₂* in the subselected voxels with 60–100% short T₂* components

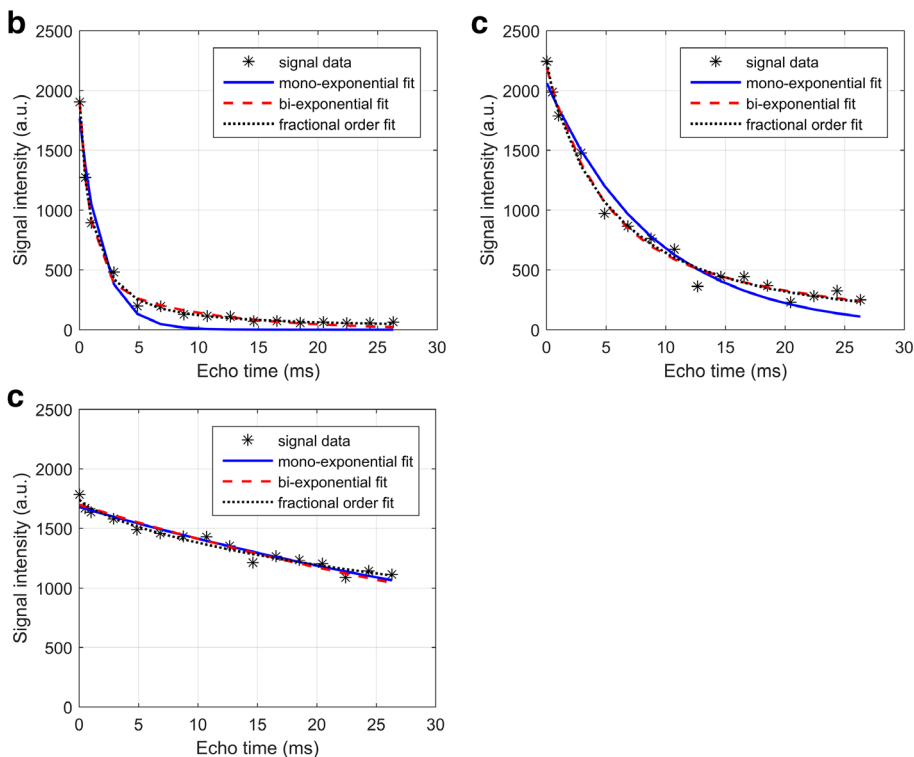
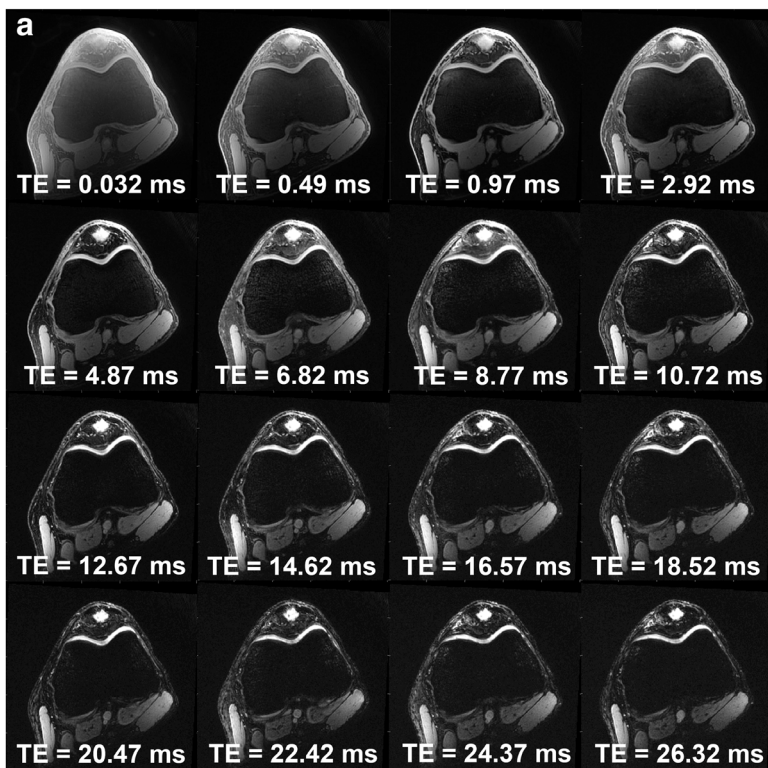


FIGURE 3: Axial 3D UTE-Cones images of the knee and corresponding T_2^* relaxation curves. (a) Axial images of the knee in a 21-year-old male basketball player with patellar tendinopathy at all 16 echoes acquired using the 3D UTE-Cones acquisitions. Note that the signal in the voxels corresponding to aligned collagen in the patellar tendon rapidly decays, and is not visible anymore on images with TEs of 4.87 msec and longer. (b) Signal intensity curves for an ROI in voxels containing mostly short T_2^* components (aligned collagen). Note that there is significant residual signal that is not fitted by the monoexponential model and that there is visibly improved curve fit of the signal data when using the biexponential or fractional order model. (c) Signal intensity curves for an ROI in voxels containing intermediate T_2^* components (interface between aligned collagen and degenerative tissue). (d) Signal intensity curves for an ROI in voxels containing mostly long T_2^* components (degenerative tissue).

TABLE 3. Measurements Resulting From Monoexponential, Biexponential, and Fractional Order Fitting of JTE Images of the Proximal Patellar Tendon, Using Voxelwise T₂* Relaxation Data for All Slices and for Each Individual Slice Combined for 65 Subjects (20,000–250,000 Voxels)

	Monoexponential		Biexponential		Fractional order	
	T ₂ *	T _{2S} *	T _{2L} *	% T _{2S} *	T ₂ *	α
All slices	6.43 [4.32–8.55]	1.160 [0.909–1.325]	15.10 [13.73–16.96]	52.9 [35.5–69.6]	4.39 [3.06–5.78]	0.829 [0.809–0.845]
Slice 1	10.39 [7.71–12.38]	0.947 [0.710–1.112]	17.64 [15.10–21.15]	32.5 [25.4–49.2]	7.69 [4.78–9.49]	0.816 [0.797–0.839]
Slice 2	9.58 [6.65–11.49]	0.906 [0.734–1.109]	17.29 [14.83–20.54]	37.1 [26.8–54.0]	6.62 [4.09–8.68]	0.811 [0.790–0.836]
Slice 3	8.51 [5.65–10.15]	0.938 [0.731–1.114]	15.94 [14.51–19.34]	36.4 [30.2–60.8]	5.84 [3.36–7.42]	0.821 [0.793–0.838]
Slice 4	7.28 [4.50–9.74]	1.010 [0.778–1.197]	15.17 [13.51–18.07]	41.6 [31.5–62.4]	5.00 [3.19–7.02]	0.824 [0.796–0.840]
Slice 5	6.50 [4.18–9.13]	1.072 [0.771–1.352]	14.80 [12.85–16.95]	45.4 [36.0–67.0]	4.48 [3.01–6.30]	0.831 [0.807–0.847]
Slice 6	5.96 [4.11–7.71]	1.177 [0.883–1.418]	14.23 [12.46–16.01]	53.1 [35.9–69.4]	4.25 [2.89–5.79]	0.832 [0.811–0.852]
Slice 7	5.58 [3.81–7.19]	1.259 [0.943–1.511]	13.91 [12.45–16.28]	59.5 [36.6–75.8]	3.79 [2.57–5.14]	0.837 [0.815–0.852]
Slice 8	5.16 [3.54–6.49]	1.332 [0.947–1.538]	13.78 [12.33–16.43]	63.6 [42.5–80.5]	3.47 [2.35–4.84]	0.839 [0.820–0.856]
Slice 9	4.81 [3.32–6.02]	1.416 [1.039–1.678]	13.81 [12.28–16.75]	69.1 [47.6–81.7]	3.38 [2.26–4.47]	0.838 [0.821–0.858]
Slice 10	4.55 [3.26–5.63]	1.503 [1.203–1.734]	14.27 [12.12–17.34]	71.3 [53.9–82.8]	3.08 [2.24–4.07]	0.838 [0.818–0.857]

T₂* relaxation times are expressed as median ± IQR in msec.

T_{2S}*: short T₂* relaxation time; T_{2L}*: long T₂* relaxation time; %T_{2S}*: percentage of short T₂* components.

T_{2F}*: fractional order T₂* relaxation time; α: fractional order exponent.

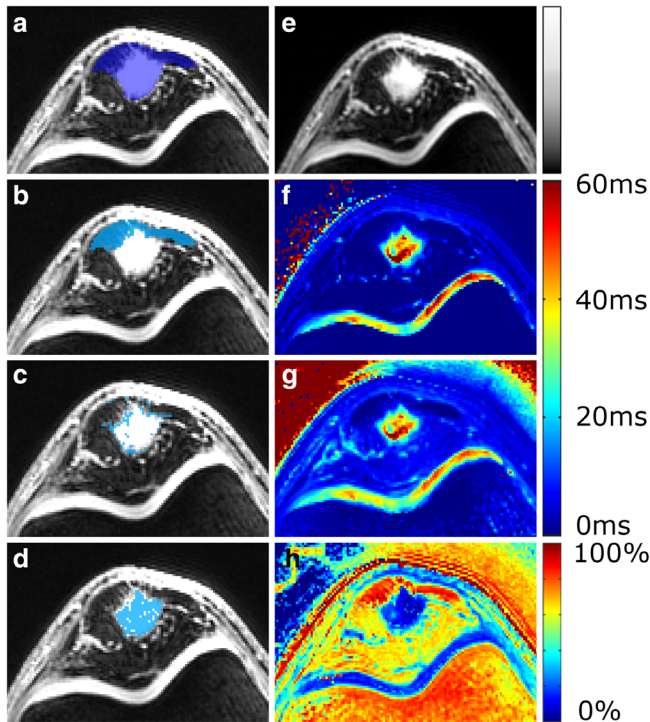


FIGURE 4: Representative axial MR images in an athlete with patellar tendinopathy. (a) Mask (blue) covering all voxels within the outer margins of the patellar tendon. (b) Subselected voxels with 60–100% short T_2^* components, corresponding to aligned collagen in the patellar tendon. (c) Subselected voxels with 30–60% short T_2^* components, corresponding to the interface between aligned collagen and degenerative tissue. (d) Subselected voxels with 0–30% short components, corresponding to degenerative tissue. (e) Original UTE image (TE 4.82 msec) revealing the regional variations of T_2^* in patellar tendinopathy, with hypointense aligned collagen and hyperintense degenerative tissue. (f) Quantitative T_2^* map from fractional order fitting, depicting short T_2^* in dark blue (0.032–10 msec) and longer T_2^* on a scale from light blue/green (10–30 msec) to orange/red (30–60 msec). (g) Quantitative T_2^* map from monoexponential fitting, on the same scale as (f). (h) Quantitative T_2^* map from biexponential fitting, depicting the percentage of short T_2^* components on a scale from dark blue (0% short T_2^* components) to red (100% short T_2^* components).

and in the subselected voxels with 0–30% short T_2^* components, respectively.

Discussion

We found that parameters resulting from biexponential fitting of UTE relaxometry data successfully led to the identification and quantification of specific tissue compartments within the patellar tendon in athletes with patellar tendinopathy and that repeatability of biexponential T_2^* quantification improved using this subregional analysis compared to the standard image analysis approach. The observed T_2^* distribution in patellar tendinopathy was not homogeneous, but revealed regional variations in binding states of water, in which aligned collagen was characterized by ultrashort T_2^* and degenerative tissue generally by long T_2^* components. Conventional

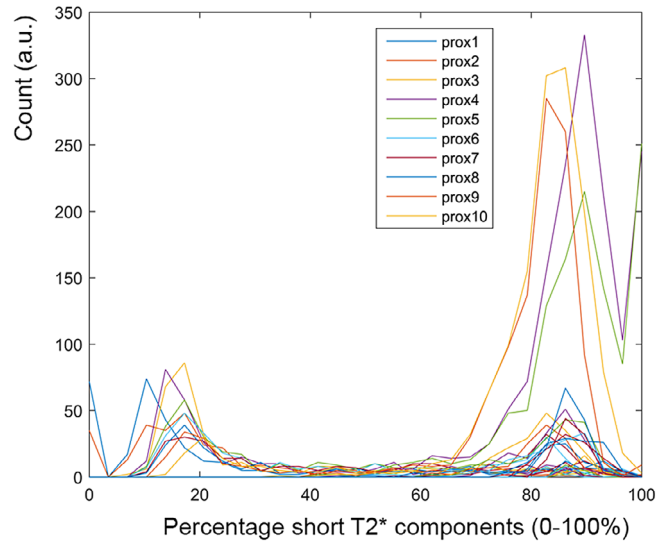


FIGURE 5: Frequency distribution of the percentage of short T_2^* components. Exemplary histogram of the frequency distribution of the percentage of short T_2^* components in the proximal patellar tendon. The different lines correspond to the manually drawn masks in 10 slices ("prox1-prox10") for T_2^* quantification. Note that there are two main peaks in the histogram, namely, the component with mostly long T_2^* (left peak) and the component with mostly short T_2^* (right peak). Based on this frequency distribution, we opted to set thresholds at 30% and 60% short T_2^* components to distinguish between three different water pools; "mostly short T_2^* (60–100% short T_2^*)," "intermediate T_2^* (30–60% short T_2^*)," and "mostly long T_2^* (0–30% short T_2^*)." Based on these thresholds on the percentage short T_2^* components, the corresponding voxels were automatically selected within each mask for analysis.

analysis with an ROI delineating the outer margins of the patellar tendon averages the spatial differences in T_2^* relaxation time in these different compartments. Accordingly, in such analyses the regional T_2^* variability complicates the detection of changes over time.

Spatial Variability in T_2^* Relaxation

To overcome the issues of spatial T_2^* variation in the patellar tendon, we introduced an alternative approach to quantify T_2^* in specific tissue compartments. This is important for identifying UTE-based biomarkers that better reflect tendon structure, other than just analyzing the average over all voxels containing different components resulting from different binding states of water. Moreover, not only spatial variability in T_2^* relaxation in the patellar tendon, but also the different components in each voxel can be quantified using biexponential fitting of UTE relaxometry data. We hypothesized that these specific biomarkers have more potential to correlate with clinical findings and hopefully better reflect the pathological changes observed in tendinopathy. Conceivably, these specific biomarkers are surrogate markers for the increased levels of glycosaminoglycans (GAGs) in patellar tendinopathy, which have already been associated with worse clinical status.¹¹

TABLE 4. Measurements Resulting From Monoexponential, Biexponential, and Fractional Order Fitting, Separated for Different Subregions of the Patellar Tendon Based Thresholds (0–30%, 30–60%, and 60–100%) on Biexponential Fitting Parameter Percentage Short T₂*

	Monoexponential		Biexponential		Fractional order	
	T ₂ *	T _{2S} *	T _{2L} *	% T _{2S} *	T _{2F} *	α
0–30%	13.78 [12.11–16.46]	0.441 [0.388–0.523]	15.79 [13.47–18.61]	20.1 [18.6–21.8]	11.82 [10.09–14.44]	0.856 [0.835–0.873]
30–60%	7.65 [6.49–8.61]	1.042 [0.751–1.507]	11.76 [10.68–13.72]	40.3 [33.6–46.8]	5.14 [4.25–5.96]	0.814 [0.789–0.828]
60–100%	3.05 [2.52–3.60]	1.693 [1.417–2.003]	17.29 [14.90–19.22]	83.2 [80.2–86.9]	2.19 [1.82–2.64]	0.828 [0.804–0.852]

T₂* relaxation times are expressed as median ± IQR in msec.
T_{2S}*: short T₂* relaxation time; T_{2L}*: long T₂* relaxation time; %T_{2S}*: percentage of short T₂* components.
T_{2F}*: fractional order T₂* relaxation time; α: fractional order exponent.

TABLE 5. Reliability of T₂* Quantification in Three Athletes With Patellar Tendinopathy

	Athlete 1		Athlete 2		Athlete 3	
	CV (%)	CR (msec)	CV (%)	CR (msec)	CV (%)	CR (msec)
T ₂ *	17.9 (17.5–18.4)	2.4 [1.4–3.9]	20.9 (20.5–21.4)	1.7 [1.0–2.9]	7.4 (7.1–7.6)	1.6 [0.9–2.5]
T _{2S} *	43.2 (41.6–44.7)	0.7 [0.3–1.3]	54.2 (27.9–55.6)	1.8 [0.9–3.3]	37.9 (36.2–39.4)	0.3 [0.1–0.5]
T _{2L} *	22.5 (21.6–23.4)	4.8 [2.5–9.7]	45.4 (44.1–46.6)	14.8 [6.1–33.1]	6.6 (6.3–6.8)	1.6 [0.7–2.7]
% T _{2S} *	24.0 (22.8–25.2)	11% [5–20]	26.2 (25.0–27.3)	16% [6–35]	14.4 (13.4–15.4)	4% [2–8]
T _{2F} *	20.2 (19.8–20.5)	2.2 [1.2–4.4]	26.4 (25.9–26.9)	1.7 [1.0–3.1]	9.8 (9.5–10.1)	1.9 [1.1–2.9]
α	4.1 (3.9–4.2)	0.05 [0.02–0.09]	5.9 (5.7–6.2)	0.08 [0.04–0.14]	3.5 (3.3–3.8)	0.04 [0.02–0.08]

CV: coefficient of variation in percentages (95% confidence interval).

CR: coefficient of repeatability in msec [IQR], except for “% T_{2S}*” where they are percentages; T_{2S}*: short T₂* relaxation time; T_{2L}*: long T₂* relaxation time; %T_{2S}*: percentage of short T₂* components; T_{2F}*: fractional order T₂* relaxation time; α: fractional order exponent.

Previous Studies

Previous studies have shown potential of bicomponent analysis to discriminate between athletes with patellar tendinopathy and healthy controls³¹ and to quantify different water pools in heterogeneous tissues.^{9,32} Also, regional T_2^* variations have been observed for the Achilles tendon³² and segmentation of the entire patellar tendon volume was performed to calculate mean T_2^* .³³ Those studies performing T_2^* quantification implemented sagittal scan planes and relatively large ROIs, probably due to time restrictions.^{31,34} We acquired UTE relaxation data in an axial oblique scan plane with a high in-plane resolution, thereby facilitating the introduced subregional quantification.

Strengths

The strengths of our study are the relatively large sample size and the homogeneity of the study population with respect to age and level of sports. We applied strict eligibility criteria by including only athletes with clinically and ultrasound-confirmed PT, and thereby ruling out other causes for anterior knee pain. Another strength is that the UTE MRI relaxation data were acquired by a single examiner using a standardized protocol, regarding both patient positioning and acquisition. Moreover, the postprocessing and analysis of the data were performed by the same investigator.

Limitations

First, the biexponential model that we used for defining the thresholds for selection of voxels with comparable water pools might be a simplified method. In fact, the MR signal in each voxel can consist of more than two (short and long) components.⁸ However, we found that the percentage of short T_2^* components was able to clearly discriminate between the different tissue compartments in the patellar tendon. Moreover, biexponential fitting has been stated to be better than monoexponential fitting, because of the systematic residual signal that is seen with monoexponential fitting.⁹ Second, the reliability of the biexponential model is relatively poor compared to the more robust monoexponential and fractional order model in the small number of subjects included for reliability measurements. However, the reliability of biexponential fitting parameters increased in specific tissue compartments compared to the conventional image analysis approach. Third, despite the noninvasiveness of MRI, the time-consuming acquisition protocol and postprocessing pipeline used in this study would both not be applicable in daily clinical practice. However, the total acquisition time of our comprehensive 3D UTE-Cones T_2^* mapping protocol can be shortened considerably by reducing the number of echoes and number of slices acquired, without compromising the T_2^* mapping results.

Further Implications

Further research projects could strengthen the need for T_2^* -quantification in specific tissue compartments in patellar tendinopathy if longitudinal data depicted changes in T_2^* relaxation over time. Subsequently, the effectiveness of different therapeutic interventions for patellar tendinopathy could be evaluated. Ultimately, imaging biomarkers would serve as surrogate markers for the increase in GAGs, thereby strongly facilitating the assessment of the severity of patellar tendinopathy at a microstructural level. Accordingly, the therapeutic response could be quantified without the need of histological samples.

Conclusion

Our study showed that quantitative multicompartiment T_2^* analysis in heterogeneous tissues such as the patellar tendon can be facilitated using a voxel selection method based on biexponential fitting parameters that differentiate between tissue compartments with comparable water pools, and that monoexponential and fractional order fitting methods have equal reliability to quantify UTE relaxometry data. Subregional quantitative analysis using 3D UTE MRI leads to the identification of tissue-specific T_2^* biomarkers with high repeatability, which can facilitate the detection of changes in the tendon hydration state over time, for example, as a result of therapeutic interventions.

Acknowledgments

The authors thank the National Basketball Association (NBA) and GE Healthcare Collaboration for providing the research grant and Michael Carl, PhD, Paul Baron, PhD, and Piotr Wielopolski, PhD, for assistance in the MRI protocol optimization.

Grant support: Financial support was provided by a research grant from a collaboration between the National Basketball Association (NBA) and GE Healthcare.

REFERENCES

1. Van der Worp H, de Poel HJ, Diercks RL, van den Akker-Scheek I, Zwerver J. Jumper's knee or lander's knee? A systematic review of the relation between jump biomechanics and patellar tendinopathy. *Int J Sports Med* 2014;35:714-722.
2. Malliaras P, Cook J, Purdam C, Rio E. Patellar tendinopathy: Clinical diagnosis, load management, and advice for challenging case presentations. *J Orthop Sport Phys Ther* 2015;45:887-898.
3. Kettunen JA, Kvist M, Alanen E, Kujala UM. Long-term prognosis for jumper's knee in male athletes. A prospective follow-up study. *Am J Sports Med* 2002;30:689-692.
4. De Vries AJ, Koolhaas W, Zwerver J, et al. The impact of patellar tendinopathy on sports and work performance in active athletes. *Res Sports Med* 2017;25:253-265.
5. Yun SJ, Jin W, Park YK, et al. Increased signal intensity at the proximal patellar tendon: Correlation between MR imaging and histology in eight cadavers and clinical MR imaging studies. *Eur Radiol* 2015;25:2976-2983.

6. Khan KM, Cook JL, Bonar F, Harcourt P, Astrom M. Histopathology of common tendinopathies. Update and implications for clinical management. *Sports Med* 1999;27:393-408.
7. Parkinson J, Samiric T, Ilic MZ, Cook J, Handley CJ. Involvement of proteoglycans in tendinopathy. *J Musculoskelet Neuronal Interact* 2011; 11:86-93.
8. Peto S, Gillis P, Henri VP. Structure and dynamics of water in tendon from NMR relaxation measurements. *Biophys J* 1990;57:71-84.
9. Chen J, Grogan SP, Shao H, et al. Evaluation of bound and pore water in cortical bone using ultrashort-TE MRI. *NMR Biomed* 2015;28:1754-1762.
10. Privalov PL, Crane-Robinson C. Role of water in the formation of macromolecular structures. *Eur Biophys J* 2017;46:203-224.
11. Attia M, Scott A, Carpentier G, et al. Greater glycosaminoglycan content in human patellar tendon biopsies is associated with more pain and a lower VISA score. *Br J Sports Med* 2014;48:469-475.
12. Chang EY, Du J, Chung CB. UTE imaging in the musculoskeletal system. *J Magn Reson Imaging* 2015;41:870-883.
13. Hodgson R, O'Connor PJ, Grainger AJ. Tendon and ligament imaging. *Br J Radiol* 2012;85:1157-1172.
14. Robson MD, Gatehouse PD, Bydder M, Bydder GM. Magnetic resonance: An introduction to ultrashort TE (UTE) imaging. *J Comput Assist Tomogr* 2003;27:825-846.
15. Vergeldt FJ, Prusova A, Fereidouni F, et al. Multi-component quantitative magnetic resonance imaging by phasor representation. *Sci Rep* 2017;7:861.
16. Chang EY, Du J, Statum S, Pauli C, Chung CB. Quantitative bi-component T₂* analysis of histologically normal Achilles tendons. *Muscles Ligaments Tendons J* 2015;5:58-62.
17. Magin RL, Li W, Pilar Velasco M, et al. Anomalous NMR relaxation in cartilage matrix components and native cartilage: Fractional-order models. *J Magn Reson* 2011;210:184-191.
18. Barber-Westin SD, Noyes FR. Assessment of sports participation levels following knee injuries. *Sports Med* 1999;28:1-10.
19. Visentini PJ, Khan KM, Cook JL, Kiss ZS, Harcourt PR, Wark JD. The VISA score. *J Sci Med Sport* 1998;1:22-28.
20. Kulig K, Landel R, Chang Y-J, et al. Patellar tendon morphology in volleyball athletes with and without patellar tendinopathy. *Scand J Med Sci Sports* 2013;23:e81-e88.
21. Klein S, Staring M, Murphy K, Viergever MA, JPM P. Elastix: a toolbox for intensity-based medical image registration. *IEEE Trans Med Imaging* 2010;29:196-205.
22. Huizinga W, Poot DHJ, Guyader J-M, et al. PCA-based groupwise image registration for quantitative MRI. *Med Image Anal* 2016;29: 65-78.
23. Du J, Diaz E, Carl M, Bae W, Chung CB, Bydder GM. Ultrashort echo time imaging with bicomponent analysis. *Magn Reson Med* 2012;67: 645-649.
24. Reiter DA, Magin RL, Li W, Trujillo JJ, Pilar Velasco M, Spencer RG. Anomalous T₂ relaxation in normal and degraded cartilage. *Magn Reson Med* 2016;76:953-962.
25. Magin RL, Ingo C, Colon-Perez L, Triplett W, Mareci TH. Characterization of anomalous diffusion in porous biological tissues using fractional order derivatives and entropy. *Microporous Mesoporous Mater* 2013; 178:39-43.
26. Poot DHJ, Klein S. Detecting statistically significant differences in quantitative MRI experiments, applied to diffusion tensor imaging. *IEEE Trans Med Imaging* 2015;34:1164-1176.
27. Andersson JLR. Maximum a posteriori estimation of diffusion tensor parameters using a Rician noise model: Why, how and but. *Neuroimage* 2008;42:1340-1356.
28. Hyslop NP, White WH. Estimating precision using duplicate measurements. *J Air Waste Manag Assoc* 2009;59:1032-1039.
29. Bland JM, Altman DG. Measurement error. *BMJ* 1996;313:744.
30. Vaz S, Falkmer T, Passmore AE, Parsons R, Andreou P. The case for using the repeatability coefficient when calculating test-retest reliability. *PLoS One* 2013;8:e73990.
31. Kijowski R, Wilson JJ, Liu F. Bicomponent ultrashort echo time T₂* analysis for assessment of patients with patellar tendinopathy. *J Magn Reson Imaging* 2017;46:1441-1447.
32. Juras V, Zbyn S, Pressl C, et al. Regional variations of T₂* in healthy and pathologic achilles tendon in vivo at 7 Tesla: Preliminary results. *Magn Reson Med* 2012;68:1607-1613.
33. Krämer M, Maggioni MB, Brisson NM, et al. T₁ and T₂* mapping of the human quadriceps and patellar tendons using ultra-short echo-time (UTE) imaging and bivariate relaxation parameter-based volumetric visualization. *Magn Reson Imaging* 2019;63:29-36.
34. Juras V, Apprich S, Szomolanyi P, Bieri O, Deligianni X, Trattinig S. Bi-exponential T₂ analysis of healthy and diseased Achilles tendons: An in vivo preliminary magnetic resonance study and correlation with clinical score. *Eur Radiol* 2013;23:2814-2822.